# The 3Bs Materials 2024 Intl. Conference

# March 06 to 08 2024, Seville, Spain

# Conference Proceedings

# Bioinspired Two Photon Polymerized Surface Textured Microstructure Antibacterial Surfaces

Georgina E. Marsh[*1,2], Ning Tan[*3], Nigel Neate[4], Keyvan Jodeiri[5], Ricky D. Wildman[5], Maxine Swee-Li Yee[6]

[1] Swansea University Medical School, Swansea University, Swansea, United Kingdom, g.e.marsh@swansea.ac.uk

[2] School of Pharmacy, Faculty of Science and Engineering, University of Nottingham Malaysia, Jalan Broga, 43500 Semenyih, Selangor, Malaysia.

[3]Department of Mechanical, Manufacturing & Materials Engineering, Faculty of Science and Engineering, University of Nottingham Malaysia, Jalan Broga, 43500 Semenyih, Selangor, Malaysia. hbynt1@nottingham.edu.my

[4]Nanoscale and Microscale Research, University of Nottingham, University Park, Nottingham NG7 2RD, United Kingdom Nigel.Neate@nottingham.ac.uk

[5]Centre for Additive Manufacturing, Faculty of Engineering, University of Nottingham, University Park, Nottingham NG7 2RD, United Kingdom. Keyvan.JodeiriIran1@nottingham.ac.uk Ricky.Wildman@nottingham.ac.uk

[6]Centre of Nanotechnology and Advanced Materials, Faculty of Science and Engineering, University of Nottingham Malaysia, Jalan Broga, 43500 Semenyih, Selangor, Malaysia. Maxine.Yee@nottingham.edu.my

*These two authors contributed equally to the work.

## Abstract

Healthcare-associated infections (HAIs) encompass all infections linked to medical procedures or exposure to healthcare environments. However, several primary risk factors for infection development are associated with the usage of implanted devices and indwelling devices. Notably, infections related to implants contribute to at least 25% of all HAIs in the US. To mitigate this risk, prophylactic antimicrobials are often required, further exacerbating the proliferation of antibiotic resistance. Consequently, there is a growing demand for surfaces capable of preventing bacterial attachment and colonization.

Numerous studies have explored the potential of natural surfaces to exhibit antibiofouling and antibacterial properties. The self-cleaning characteristics of the lotus leaf and the microstructures present on the Japanese edible crab, are renowned for deterring bacterial cell attachment, aiding in the prevention of biofilm formation. In this study, our objective is to fabricate microstructures, on a scale comparable to these natural surfaces, using a two photon polymerization 3D printer. By culturing P. aeruginosa on these surfaces we can then investigate the influence of micropillar surface characteristics on P. aeruginosa attachment or response. Biomimetic microstructures were successfully created with differing spacings and precisely controllable surface textures. The 5 µm spacing, showed to produce greater antibacterial effect. The 5 µm spacing demonstrated an improved antibacterial effect and vertical ridges on the walls of the microstructures, showed the lowest cell adhesion to the microstructures themselves, but increased clustering around their base.

**Keywords:** Two photon polymerization, biomimetic, micropillared surfaces, biofilm, antibacterial.

## 1. Introduction

Healthcare-associated infections (HAIs) impose significant challenges in medical settings, often stemming from the contamination of indwelling medical devices and prosthetic implants predominantly caused by antibiotic-resistant bacteria during invasive procedures. One in 31 hospitalised patients acquire at least one HAI at any given time, contributing to over 720,000 of HAIs and billions of dollars excessive healthcare cost in the United States each year [1]. In response to the growing need for innovative surfaces capable of preventing bacterial attachment and colonization without relying on antibiotic chemical agents, nature had inspired researchers to explore biomimetic solutions that mimic natural surfaces known for their antibacterial properties [2]. Among the various microfabrication

techniques, two-photon polymerization, a direct laser writing technique offers greater precision and controllability to fabricate complex 3D microstructures[3]. In this study we aim to fabricate controllable microstructures of a size and spacing like those seen on natural surfaces and assess their antibacterial nature.

## 2. Methodology

### 2.1 3D Design and fabrication

The micropillar structures were designed using computer-aided design (CAD) modelling software Blender 3.3.1 and DeScribe. Micropillars of varying centre-to-centre spacings (5μm and 8μm) were designed alongside three types of micropillar textured walls, herein referred to as ridgeless, vertical ridged and ringed surfaces. To fabricate the sample, acrylate photoresist (IP-L 780, Nanoscribe) was drop-casted on a 22mm × 22mm glass coverslip and subjected to the two-photon polymerization (TPP) system (Photonic Professional GT, Nanoscribe GmbH) in piezo mode. The micropillar arrays of 300 μm × 300 μm were fabricated using a laser power of 25mW; hatching distance 0.1 μm; slicing distance 0.1 μm to 0.5 μm; contour of zero to two.

### 2.2 Characterisation of 3D printed micropillars

Scanning electron micrograph of the microstructures were captured using JEOL 7000F field-emission SEM to visualize the pattern arrangement and morphological characteristics of the printed micropillars. Subsequently, the height and spacings of the micropillar were assessed using Filmetrics-Optical profilometer (Profilm3D, USA) using a 50X Nikon DI objective.

### 2.3 Bacterial response to micropillared surfaces

The biofilm biomass was quantified by the crystal violet assay as described elsewhere [4]. Refreshed culture of *P. aeruginosa* ATCC 27853 (Gram-negative) were adjusted to $OD_{600}= 0.1$ using UV-visible spectrophotometry. The micropillar array was covered in 50 μL of adjusted bacterial suspension and incubated at 37 °C for 24 h. A flat control was used to compare bacterial cell attachment and biofilm-forming capacity on micropillars and flat surfaces. Furthermore, SEM imaging was also performed on fixed micropillar array post incubation with *P. aeruginosa* to assess their morphology and surface attachment behaviour. The samples were fixed with 4% paraformaldehyde followed by dehydration with a series of ethanol and hexamethyldisilazane solutions.

## 3. Results and Discussion

The optical profilometry (Figure 1 (a)-(b)) showed that micropillars of height ~4.5 μm and diameter of ~3 μm were successfully fabricated, with centre-to-centre spacings consistent with the 3D computer-aided design. Micropillars with centre-to-centre spacings of 5 μm (i.e., interspacing of ~ 2μm) and 8 μm (interspacing of ~5 μm) showed a significant reduction in bofilm formation as opposed to the flat surface (ANOVA, P=0.002 for 5 μm; P=0.014 for 8 μm, P<0.05). Micropillar with centre-to-centre spacings of 5 μm showed slightly greater antibiofilm capability as opposed to the 8 μm spaced pillars, however, statistical analysis showed no significant differences (ANOVA, P = 0.189, P < 0.05) between the 8 μm topography and 5 μm topography. Previous studies have shown that surface topography can limit bacterial cell adhesion to the surface, particularly evident with reduced spacings between the pillars [5]. Suggesting that smaller spacings in our study likely resulted in the reduced settlement of bacteria within the interstitial space of the micropillars. Bacterial settlement on the surface precedes biofilm formation, a higher density of bacterial cells adhering to the surface could lead to the formation of a denser biofilm.
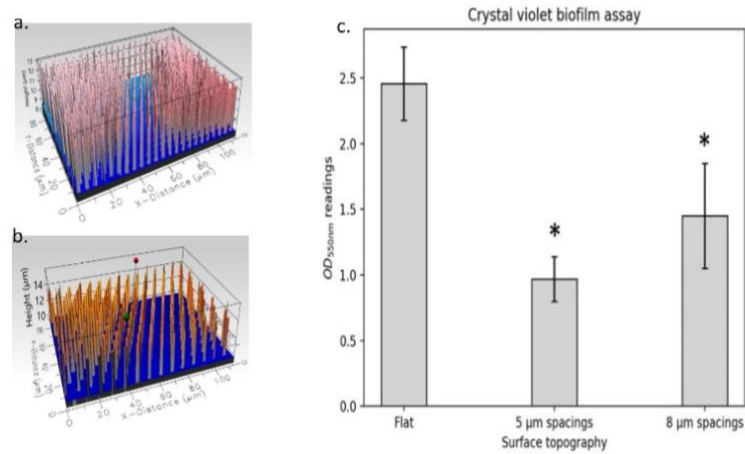
**Figure 1**: Optical profilometry of micropillars of (a) 5 µm spacings; (b) 8 µm spacings. (c) An overview of the mean OD at 550 nm (± standard deviation) representing the P. aeruginosa bacteria biofilm attachment on 5 µm and 8 µm spaced topographies compared to flat control surface in triplicates. Bars represent mean OD measured at 550 nm±s.d. of three independent experiments. * indicate statistical significance compared to control (P<0.05).

The hexagonal pattern arrangement of micropillar structures is shown in Figure 2(a)-(c). The consistent centre-to-centre spacings of 5 µm were maintained for subsequent bacterial testing to examine the impact of differing wall texture on bacterial cells attachment behaviour. The cross-section SEM image confirmed that micropillars of varying wall textures (vertical ridged and ringed surfaces) were formed by hatching and slicing of the structure at varying distances as it is controlled by the laser trajectory. Smooth ridgeless wall texture was fabricated by adding more than one contour line for each sliced layer with distance between the lines set at 0.1 µm. Micropillars fabricated with ridgeless and vertical ridged surfaces maintained their position and structural integrity during washing. In contrast, micropillars with ringed surface appeared to have weaker structural integrity and a few structures toppled over during washing.
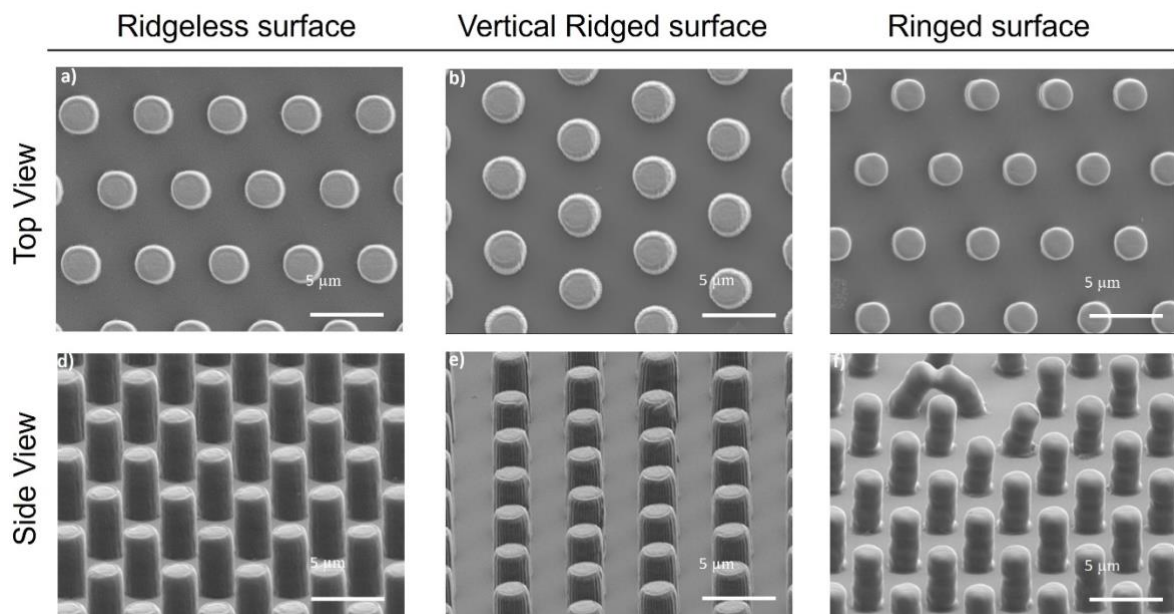


**Figure 2** SEM images x5000 magnification of micropillar structures with varying surface texture characteristics formed by TPP (a)-(c) Top view SEM image; (d)-(f) Cross-section SEM image captured at 60° tilt angle.

With consistent centre-to-centre micropillar spacings of 5 µm, the interplay between bacterial cells and micropillars of varying wall textures were investigated using SEM. Figure 3 illustrates bacterial cell density on the micro topographical array, showing lowest adherence of cells on micropillar walls

textured with vertical ridges, but increased clustering around their base (Figure 3(c)). Conversely, ridgeless and ringed texture showed higher proportion of cells adhered on their walls.
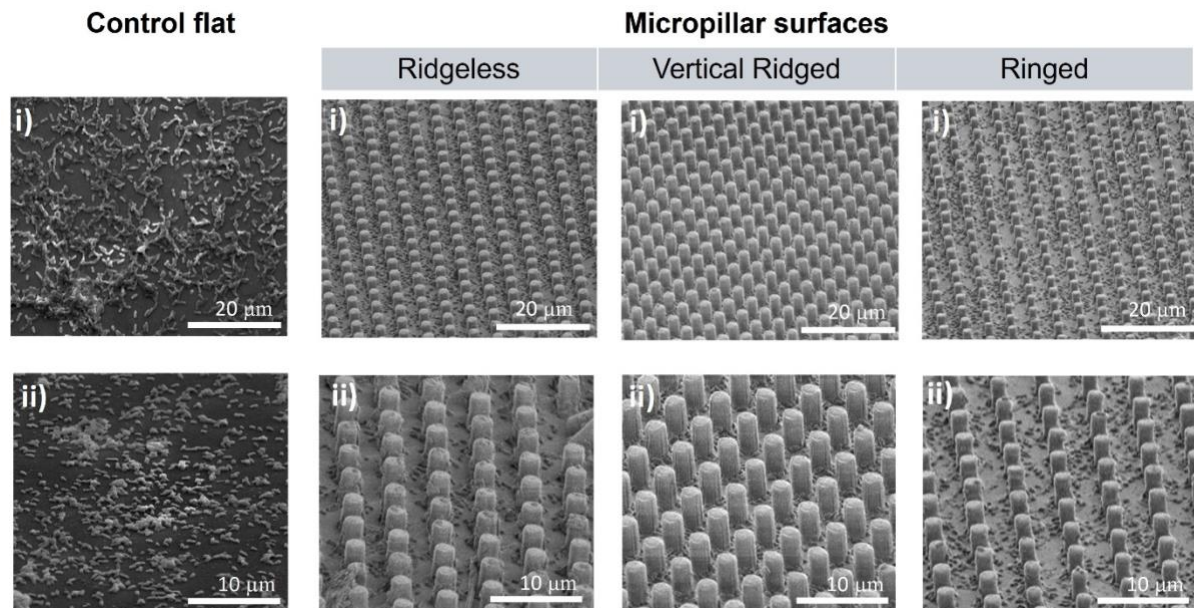


**Figure 3** SEM images of P. aeruginosa on (a) flat control surface; (b)-(d) micropillars of varying wall surface texture under (i) ×5000 and (ii) ×10000 magnifications.

## 4.    Conclusion

In summary, the interaction between micropillar wall texture and attachment of bacterial cells is mainly dependent on the surface texture of the micropillars. Smooth textured micropillar walls and micropillar walls with ringed texture promoted the attachment of P. aeruginosa, while micropillars with vertical ridged walls deterred biofilm formation. In fact, bacteria tended to aggregate around the base of these micropillars instead. These intriguing results serves to inform future work on the next generation of antibacterial surface materials.

### Acknowledgements

### References

1.  S. S. Magill *et al.*, "Changes in Prevalence of Health Care–Associated Infections in U.S. Hospitals," *N. Engl. J. Med.*, vol. 379, no. 18, 2018, doi: 10.1056/nejmoa1801550.
2.  J. Hasan, S. Jain, R. Padmarajan, S. Purighalla, V. K. Sambandamurthy, and K. Chatterjee, "Multi-scale surface topography to minimize adherence and viability of nosocomial drug-resistant bacteria," *Mater. Des.*, 2018, doi: 10.1016/j.matdes.2017.11.074.
3.  D. Schwärzle, X. Hou, O. Prucker, and J. Rühe, "Polymer Microstructures through Two-Photon Crosslinking," *Adv. Mater.*, vol. 29, no. 39, 2017, doi: 10.1002/adma.201703469.
4.  E. Peeters, H. J. Nelis, and T. Coenye, "Comparison of multiple methods for quantification of microbial biofilms grown in microtiter plates," *J. Microbiol. Methods*, vol. 72, no. 2, 2008, doi: 10.1016/j.mimet.2007.11.010.
5.  X. Ge *et al.*, "Bacterial responses to periodic micropillar array," *J. Biomed. Mater. Res. - Part A*, vol. 103, no. 1, 2015, doi: 10.1002/jbm.a.35182.

# Fabrication and Characterization of Gallic Acid-Loaded Poly (lactic acid) Electrospun Fibers for Tissue Engineering Applications

Nuttawut Sribungngaw[1], Parichart Naruphontjirakul[1], Poommaree Namchaiw[1],
Kamolchanok Ngamkham[1]

[1]Biological Engineering Program Faculty of Engineering King Mongkut's University of Technology Thonburi. 126 Pracha Uthit Rd., Bang Mod, Thung Khru, Bangkok 10140, Thailand.
Email: Nuttawut.srib@kmutt.ac.th

**Abstract**

The main property of a bioactive scaffold is not only to provide an extracellular matrix but also to accelerate tissue regeneration. Thus, the addition of bioactive compounds to the scaffolds becomes a key method to increase the potential of tissue-engineered scaffolds. In this work, poly(lactic acid)(PLA) nanofibrous scaffolds incorporated with various concentrations of gallic acid (GA) (0, 2.5, 5, and 10 mg/ml) were prepared by electrospinning. The scaffold properties were assessed through SEM imaging, GA releasing assay, and degradation assay. SEM imaging revealed that the set-up electrospinning condition can be used to fabricate gallic acid-loaded nanofibers and the incorporation of GA did not have a discernible impact on the average fiber diameter and morphology. In addition, the release of GA increased with respect to GA content of the fibers. The degradation assays indicated that the weight of the scaffolds reduced over time but more than 80% of the fiber mass remained after 28 days in all formulations. In summary, the preliminary results of this research suggest that PLA electrospun fibers incorporated with GA hold general properties of bioactive scaffolds which can be further studied as a tissue-engineered construct.

**Keywords:** Gallic Acid, PLA Electrospun Fiber, Regenerative Medicine, Tissue Engineering

## 1. Introduction

The incidence of bone defects increases over time, especially when aging society becomes a global trend. Although autologous and allogeneic bone grafts are being established as the primary consideration for treatment, graft insufficiency remains a significant limitation [1]. Despite biomimetic sciences having been studied for a relatively short period, bone tissue engineering has rapidly emerged as a groundbreaking approach in the field of regenerative medicine. It is considered as an alternative treatment which could overcome the limitations of the conventional therapeutic approaches. Biodegradable polymers such as poly(lactic acid) (PLA) have been widely utilized to fabricate scaffolds, particularly through electrospinning, due to their excellent biocompatibility, good mechanical properties, ability to promote cell adhesion, and biodegradability. Beyond the use of biodegradable polymers, the incorporation of bioactive compounds to the scaffold further enhances the regenerative or differentiation properties [2]. Gallic acid (GA), a prevalent phenolic acid in plants, is known for its antioxidant properties and other potential health benefits. GA and its derivative, 4-O-methylgallic acid, have shown positive effects on osteoblast differentiation and bone tissue development [3]. The studies in rats demonstrated enhanced bone healing and osteogenic differentiation when GA-loaded chitosan particles were applied [4], [5]. However, the interaction between GA-releasing scaffolds and bone stem cells has not been investigated yet. Therefore, in this study, different concentrations of GA were incorporated into PLA and fabricated using electrospinning technique. The obtained scaffolds were characterized and assessed its potential in tissue engineering applications using SEM imaging, GA release assay, and degradation assay.

## 2. Materials and Methods

### 2.1. Scaffold Fabrication

The fibrous scaffolds were divided into four formulations with respect to GA content, namely GA0, GA2.5, GA5, and GA10 (representing GA concentrations of 0, 2.5, 5, and 10 mg/ml, respectively). The total polymer concentration of 12% w/v was prepared by dissolving PLA (MW=100,000)(NatureWorks) in chloroform: methanol (4:1). GA was added to the dissolved PLA according to the respective formulations. The solutions

from each formulation were then electrospun under the following parameter settings: a distance from the tip to the collector of 13 cm, electrical voltage of 13 kV, and injection rate of 1 ml/hr.

## 2.2. SEM Imaging

Morphology of the scaffolds were observed by SEM (JSM-6610LV, JOEL, serviced by the Department of Tool and Materials Engineering, King Mongkut's University of Technology Thonburi (KMUTT)). The fibers were sputter-coated with gold before imaging. The images were snapped at 1000x and 5000x magnification from at least three distinct zones. The fiber diameters were measured using ImageJ software.

## 2.3. GA Release Assay

The release of GA was assessed through an *in vitro* drug release assay conducted in 1x phosphate buffer saline (PBS). Fiber sheets, 4×4 cm², were immersed in a 15 mL tube containing 12 mL of PBS. The PBS solution enriched with GA were collected and absorbance readings were taken at 260 nm using a microplate reader at specific time points (1 hr, 8 hr, 24 hr, 3 days, 6 days, 9 days, 12 days, and 15 days). The PBS was renewed at each time point, and the released amount of GA was normalized with their individual weights.

## 2.4. Degradation Assay

To assess scaffold degradation in a static setting, the fiber sheet 6×5 cm$^2$ from each condition was sterilized and incubated in a 15 ml centrifuge tube containing 10 mL of 1xPBS. The samples were incubated at 37ºC for a maximum of 28 days. The PBS solution was entirely renewed every 3 days. Dry weight loss was measured every 7 days and calculated for % weight loss using equation (1). Where $M_0$ is the initial weight of the fiber sheet. $M_D$ is the dry weight of the fiber sheet after degradation.

$$\text{Weight loss (\%)} = \frac{M_0 - M_D}{M_0} \times 100 \qquad (1)$$

## 2.5. Statistic Analysis

Data normality was assessed using a Shapiro-Wilk test. Statistical differences between groups were evaluated using ANOVA followed by Tukey's post hoc test. A significance level of $p < 0.05$ was applied to determine any differences for all analyses. R Studio was utilized for statistical calculations. All data were shown as mean ± SD.

## 3. Results and Discussions

## 3.1. SEM Imaging

SEM imaging revealed randomly arranged fibers forming mats in all formulations (Fig.1). Nano-scale fibers were obtained without bead formation (Fig. 2), indicating appropriate electrospinning settings. The diameters of GA0, GA2.5, GA5 and GA10 formulations were $0.621 \pm 0.273$, $0.659 \pm 0.180$, $0.646 \pm 0.157$, and GA10 $= 0.656 \pm 0.186$ µm respectively. Comparison between GA0 and others indicated similarity in diameters, suggesting that GA incorporation did not significantly affect solution properties [6], [7]. Furthermore, porous structure was observed in all formulations. The porous structure observed in the mats holds significant implications for the scaffolding application. Porosity influences their key characteristics such as surface area, permeability, and mechanical properties. Therefore, the presence of pores offers advantages in terms of increased surface area for interactions, enhanced gas and fluid transport properties, and improved cell infiltration, especially in tissue engineering applications [8].
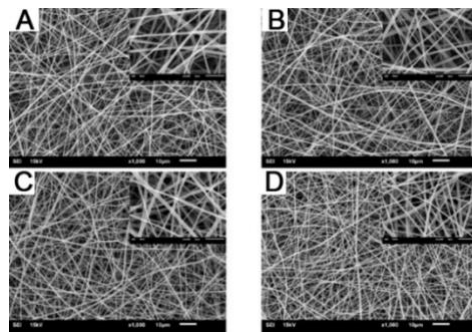
**Fig. 1**: Microstructure of the electrospun fibers; GA0 (A), GA2.5 (B), GA5 (C), GA10 (D). SEM imaging at 1000x and 5000x (top right, each) showed multiple fibers with random alignment varying in fiber size.
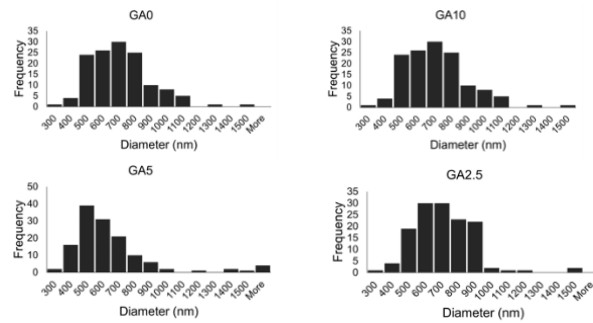
**Fig. 2**: Histograms showed the distribution of fiber's diameter in all formulations. The diameter sizes were varied and almost limited in nanoscale.

## 3.2. GA Release Assay

The controlled and sustained release of GA from the fiber mat is crucial for achieving the osteogenic induction effect, hence, GA release at different time points was quantified. The release of GA from the fibers increased according to the concentration of the incorporated GA (Fig. 3). Burst release was observed in all formulations during the first hour, possibly due to the release of GA which was coated on the fiber surface [8]. This was followed by a gradual decline of the GA release to undetectable levels. The shortest release duration was found within 3 days by GA2.5, followed by GA5 in 6 days, while GA10 showed a longer release duration of up to 9 days. After day 9, no detectable release of GA was observed in any of the formulations. Cumulative GA amount at the last detectable days of GA2.5, GA5, and GA10 were $4.23\pm0.07$, $7.67\pm0.01$, and $20.87\pm0.02$ µg GA/mg scaffold respectively. This indicates that GA-loaded electrospun scaffolds could sustained the released and delivered GA according to their GA content in the fibers.
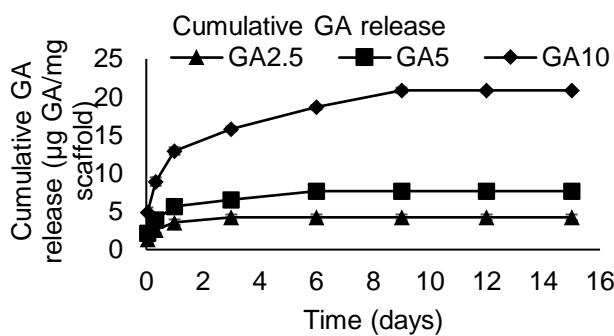




**Fig.3**: Cumulative GA release. The figure illustrates the cumulative release of GA from electrospun fibers under four conditions (GA0, GA2.5, GA5, GA10) at various time points. Burst release was observed within the first hour.
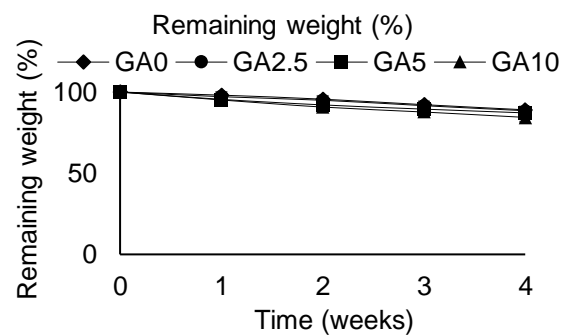
**Fig.4**: Scaffold degradation in vitro. The remaning weight(%) of the fibers in 4 formulations at day 7, 14, 21 and 28.

## 3.3. Degradation Assay

The biodegradable scaffold functions as a temporal structure that can be degraded and eventually replaced by natural tissue. Therefore, a degradation assay is crucial to confirm that the scaffold is degraded at an appropriate rate. The degradation process initiated in the first week and progressively continued, exhibiting a trend of ongoing degradation until the last week of the detection period (day 28) **(Fig.4)**. The incorporation of GA to the scaffold appeared to elevate the degradation rate in concerning to GA content, although the differences were not statistically significant. Specifically, the remaining weight percentages were as follows: GA0 = $89.05\pm0.77\%$, GA2.5 = $88.49\pm0.48\%$, GA5 = $87.17\pm1.63\%$, and GA10 = $84.39\pm1.58\%$. These degradation patterns were compatible with a surface erosion mechanism [9]. This result suggests that the

scaffolds can uphold their 3D structure for at least 28 days, indicating their suitability for long-term implantation and tissue regeneration.

## 4. Conclusion

Gallic acid-loaded PLA fibers can be obtained using electrospinning technique. SEM images exhibited broad-size nanofibers with porous architecture in GA0, GA2.5, GA5, and GA10 formulations. GA release assay indicates that GA could be released from the scaffold and sustained for a certain period according to the amount of the incorporated GA. Moreover, the degradation assay confirmed that the scaffold could maintain its 3D structure for at least 28 days. In summary, the scaffolds show promising material properties for a bioactive scaffold. However, confirmation of their biocompatibility and osteogenic potential is needed to be assessed to ensure their suitability in tissue engineering applications, particularly in bone regeneration.

## 5. Acknowledgement

## References

1. N. Xue *et al.*, "Bone Tissue Engineering in the Treatment of Bone Defects," *Pharmaceuticals*, vol. 15, no. 7, p. 879, Jul. 2022, doi: 10.3390/ph15070879.
2. A. Gregor *et al.*, "Designing of PLA scaffolds for bone tissue replacement fabricated by ordinary commercial 3D printer," *J Biol Eng*, vol. 11, no. 1, p. 31, Dec. 2017, doi: 10.1186/s13036-017-0074-3.
3. "Gallic Acid Derivative Stimulate Osteogenic Differentiation by Regulating Autophagy via JNK/mTOR Signaling Pathways in vitro," *FMSR*, vol. 3, no. 1, 2021, doi: 10.25236/FMSR.2021.030106.
4. Y. Oh, C.-B. Ahn, M. P. C. K. Marasinghe, and J.-Y. Je, "Insertion of gallic acid onto chitosan promotes the differentiation of osteoblasts from murine bone marrow-derived mesenchymal stem cells," *International Journal of Biological Macromolecules*, vol. 183, pp. 1410–1418, Jul. 2021, doi: 10.1016/j.ijbiomac.2021.05.122.
5. P. S. Kaparekar, S. Pathmanapan, and S. K. Anandasadagopan, "Polymeric scaffold of Gallic acid loaded chitosan nanoparticles infused with collagen-fibrin for wound dressing application," *Int J Biol Macromol*, vol. 165, no. Pt A, pp. 930–947, Dec. 2020, doi: 10.1016/j.ijbiomac.2020.09.212.
6. H. Fong, I. Chun, and D. H. Reneker, "Beaded nanofibers formed during electrospinning," *Polymer*, vol. 40, no. 16, pp. 4585–4592, Jul. 1999, doi: 10.1016/S0032-3861(99)00068-3.
7. M. Herrero-Herrero *et al.*, "Influence of chemistry and fiber diameter of electrospun PLA, PCL and their blend membranes, intended as cell supports, on their biological behavior," *Polymer Testing*, vol. 103, p. 107364, Nov. 2021, doi: 10.1016/j.polymertesting.2021.107364.
8. J. M. Ameer, A. K. Pr, and N. Kasoju, "Strategies to Tune Electrospun Scaffold Porosity for Effective Cell Response in Tissue Engineering," *J Funct Biomater*, vol. 10, no. 3, p. 30, Jul. 2019, doi: 10.3390/jfb10030030.
9. D. Puppi and F. Chiellini, "Drug release kinetics of electrospun fibrous systems," in *Core-Shell Nanostructures for Drug Delivery and Theranostics*, Elsevier, 2018, pp. 349–374. doi: 10.1016/B978-0-08-102198-9.00012-0

# Engineered anisotropic interlocking interface strategy for interface toughening in 3D printed bi-material thermoplastic polymers

Laia Farràs-Tasias[1], Jules Topard[2,3], Stéphane Panier[3], Francisco A. Gilabert[1], Flávio H. Marchesini[1]

[1]Department of Materials Textiles, and Chemical Engineering, Ghent University
Campus Ardoyen, Technologiepark-Zwijnaarde, Ghent, Belgium, laia.farrastasias@ugent.be
[2]College et Énergie, UniLaSalle
Quai de la Somme 14, Amiens, France
[3]Laboratoire des Technologies Innovantes, Université Picardie Jules Verne
Rue Baudelocque 15, Amiens, France

**Abstract**

This research presents an innovative strategy to enhance the interface toughness of 3D-printed bi-material thermoplastic polymers. A combination of additively manufactured materials with dissimilar mechanical properties, namely Polylactic Acid (PLA) as the stiff material and Thermoplastic Polyurethane (TPU) as the flexible material is employed. Understanding the interface generated between the two different materials is crucial to provide a solution that enhances the mechanical properties of this weak region. In this work, an increase in the performance of the interface is achieved by mechanically interlocking the rasters of the two different materials, generating an entanglement region. Three designs at different orientations are studied. Mechanical tests and optical microscopy are employed to evaluate and compare their performance.

**Keywords:** Multi-material 3D printing, interlocking interface, mechanical bonding, interface toughening

## 1. Introduction

Additive manufacturing (AM) enables the fabrication of complex geometries impossible to manufacture with traditional methods such as injection moulding. In particular, Fused Filament Fabrication (FFF) is a technique that consists of extruding a polymer through a heated nozzle to generate the desired geometry [1]. Multi-material 3D printing is achieved when printing with multiple materials for a single application [2]. The combination of materials with dissimilar mechanical properties enables the creation of components that can bend, stretch, or compress and can be useful for applications in the fields of soft robotics, medical prosthetics, and biomedical engineering, among others [3-5]. However, it is of high importance to understand the interaction between the materials employed. PLA is valued for its low environmental impact and provides rigid-like mechanical properties while TPU is known for its significant elasticity and deformability [6]. These materials can be 3D printed for multi-material applications. However, since there is low chemical compatibility between PLA and TPU, the area of contact between the materials will generate an interface with low adhesion, which may result in an area where mechanical failure is more likely to be encountered [7,8]. This research addresses the issue of weak interfaces between PLA and TPU through mechanical interlocking of the rasters. Different interfaces are designed and strategically oriented with respect to the crack propagation to effectively increase the interface toughness.

## 2. Methodology

### 2.1. Materials and Machinery

Commercial Makerfill PLA filament was purchased from 3D&I BV (Kontich, Belgium), and Polymaker PolyFlex TPU 95 was purchased from 3D Jake Nederland (Paldau, Austria). Specimens were printed in a custom-made multi-nozzle 3D printer and tested with an Instron Universal Machine. For the optical microscopy, a Keyence optical microscope was utilized.

### 2.2. Interlocking strategy and nomenclature

Specimens are designed following the design specifications of ASTM D5528, with a width of 20 mm, a total height of 4 mm (from which 2 mm of PLA and 2 mm of TPU), and a total length of 125 mm. There is an initial crack of 63 mm, and the rest of the specimen contains the interface between the two materials.

For the design of the different interfaces, two approaches have been taken into consideration. The first approach (Design A) is a unidirectional approach, in which the rasters are aligned in the same direction creating an anchor-like shape. The second approach is applied in designs B and C and consists of a cross-plied design that is inspired by textiles. In this case, the two constituent rasters of the interface, are in a perpendicular direction to each other.

The nomenclature of the specimens consists of first the letter that determines the design, and then the orientation of the interface design to the X-axis (see Fig. 1). Since it is an anisotropic design, it is orientation dependent, so 0º, 45º, and 90º angles are considered. As seen in Fig. 1, since design A is a unidirectional design, the 3 possibilities of angles are possible. However, for the cross-plied designs (B and C), only 2 configurations are possible (±45º, and 90º/0º).
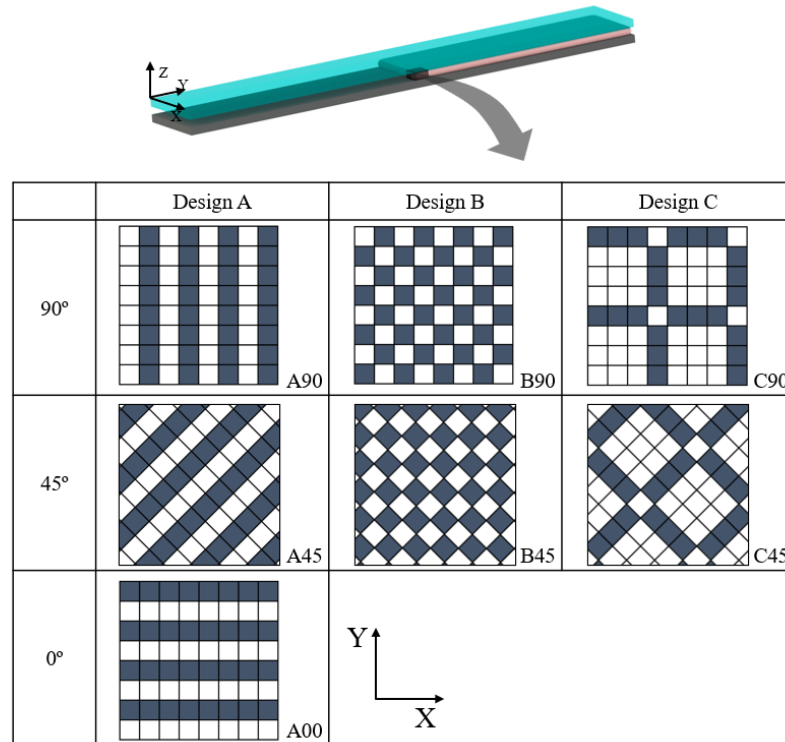


**Fig. 1**: Top: General geometry of the printed specimen. Table: Different design patterns and nomenclature of all studied designs and configuration.

## 2.3. Interfacial Strength Evaluation

In order to mimic the natural action of detaching the interface, a combination of double cantilever beam test (ASTM D5528) and 90-degree peel test (ASTM D6862) is made. The specimen is tested in a tensile machine until 35 mm of the interface are opened. In terms of evaluation, two main parameters are evaluated to compare the different interface designs. The first one is the initial force [N], required to initiate the crack in the interface, and the other parameter is an alternative definition of interface toughness. Its definition follows the equations below:

$$U = \int_{\delta_{0\ mm}}^{\delta_{x\ mm}} F(\delta) \cdot d\delta = [J] \tag{1}$$

$$G = \frac{U}{\delta_{end} \cdot w} = \left[\frac{J}{mm^2}\right] \tag{2}$$

The integration corresponds to the area under the testing curve (see Fig. 2). Our definition of interface toughness takes into consideration the span required to obtain 35 mm of crack propagation in the interface. Testing nomenclature is also indicated in the figure.
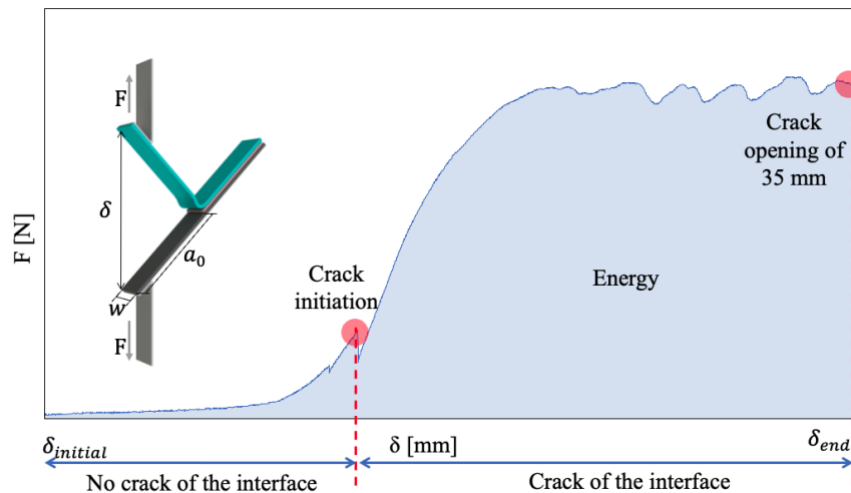
**Fig. 2**: Example of a testing curve and indication of the crack initiation force, and crack opening. Specification of the nomenclature and indication of the pulling forces.

## 3. Results and discussion

Double cantilever beam-like tests (see Fig. 3) show the force required to crack 35 mm of interface of each specimen. A pattern is observed in the force-displacement plot. All specimens show an increase in force at the beginning of the test. During this increase curve, the specimen starts opening but the interface is still undamaged. The finish point of the ramp is the initial crack force, being the point where a crack in the interface is initiated. After this initiation, different behaviours can be observed depending on the design and the orientation of that design with respect to the pulling force. It is noted that compared to the pristine case (no interface between the two materials), all interface designs provide higher initial pulling forces and tougher interfaces. Nevertheless, the two designs providing the best response correspond to designs A00 and B45. When observing design A00, it is noted in the force-displacement curve that every time an "anchor" is found, there is an initial force to break this anchor, and then once it is broken, a decrease in the force until another anchor is found, that the cycle is repeated. This behaviour of preventing the crack from propagating along the interface is also seen in design B45, in which a continuous force to crack the interface is required because of the impediment of crack propagation. In this case, it is the continuous entanglement of the rasters and the orientation of the design that prevents the crack from expanding, generating a smoother curve. In terms of microscopy, there is a high accuracy in the printing process, providing interfaces that comply with the designs described.
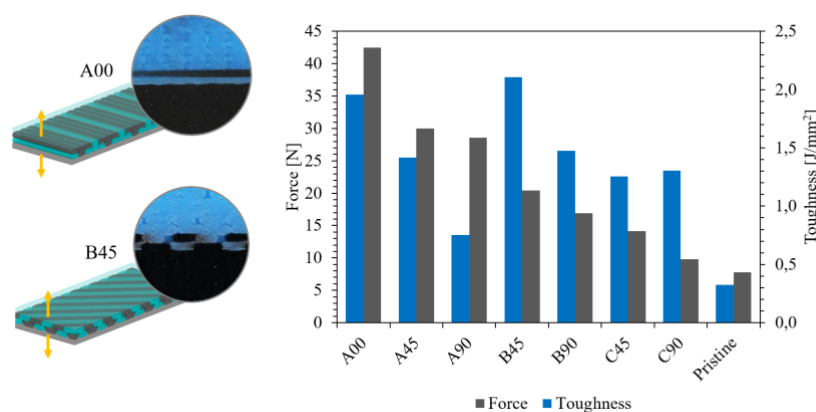


**Fig. 3**: Left: Interfaces and section images corresponding to the two best-performing specimens. Right: indication of the initial crack force [N] and interface toughness [J/mm2].

## 4. Conclusions

Specimens were successfully printed accurately following the designs described. An alternative definition for the interface toughness is provided and used to compare the different interfaces. After mechanically testing the

specimens, it is found that any interface provides better results than a pristine interface (with no entanglement). The geometry that provides the best results corresponds to Design A (the anchor-like design), oriented at 0 degrees with respect to the X-axis, providing an increase in the initial crack force of 446% and an increase in toughness of 501% compared to the pristine specimen.

Further study is being conducted for other printing orientations and the effect of friction on the performance of the different designs.

### Acknowledgements

### References

1. Chen, J., Smith, D.E.: Filament rheological characterization for fused filament fabrication additive manufacturing: A low-cost approach, Additive Manufacturing, 47 102208 (2021)
2. Shahbazi, M., Jäger, H., Ettalie, R., Mohammadi, A., Kashi, P. A.: Multimaterial 3D printing of self-assembling smart thermos-responsive polymers in 4D printed objects: A review, Additive Manufacturing 71 103598 (2023)
3. Xue, W., et. Al: Rigid-flexible coupled origami robots via multimaterial 3D printing, Smart Materials and Structures (33) 035004 (2024)
4. Hisham, M., Salih, E. A., Butt, H.: 3D printing of Multimaterial Contact Lenses, ABS Biomaterials Science and Engineering (9,7) 4381-4391 (2023)
5. Soreni-Harari, M., St. Pierre, R., McCue, C., Moreno, K., Bergbreiter, S.: Multimaterial 3D printing for micro robotic mechanisms, Soft Robotics 59-67 (2020)
6. Darnal, A., Shahid, Z., Deshpande, H., Kim, J., Muliana, A.: Tuning mechanical properties of 3D printed composites with PLA: TPU programmable filaments, Composite structures, 318, 117075 (2023)
7. Altuntas, U., Coker, D., Yavas, D., Creating tougher interfaces via suture morphology in 3D-printed multi-material polymer composited by fused filament fabrication, Additive manufacturing, 61, 103359 (2023)
8. Cañas, J., Justo, J., París, F., Evaluation of the interlaminar fracture toughness on composite materials using DCB test on symmetric and unsymmetric configurations, Composite Structures, 297, 115944 (2022)

# Evaluation of the bacterial cellulose as a green and sustainable material for fruit preservation

Chiu-Mei Kuo[1,*], Shao-Qian Huang[1], Bo-Chen Shi[1], Yan-Rong Chang[1], Yu-Tso Chen[1]

[1] Department of Chemical Engineering, Chung Yuan Christian University
No.200 Zhongbei Rd., Zhongli Dist., Taoyuan City 320314, Taiwan

## Abstract

Evaluate the preservation effect of bacterial cellulose (BC) membrane produced by adding glycerol when applied to crack-free and cracked tomatoes. The maximum BC production, BC wet membranes, and tensile strength were obtained as 1% glycerol addition in the HS medium were 1855 mg/L, 5.7 mm, and 224.5 MPa, respectively. There were more fibers and the fibers were more densely intertwined due to the higher BC production, which may lead to smaller BC pore size. The result of water vapor transmission rate (WVTR) shows that the BC membrane produced by 1% glycerol was a minimum WVTR of 266.8 $g/m^2/day$. The skin of non-cracked and cracked tomatoes without packaging began to shrink significantly from 21 days and 14 days respectively, while tomatoes packaged with BC membrane produced from 1% glycerol were similar to tomatoes packaged at initial 0 days. When using BC membrane to package tomatoes, the total plate count was reduced. The significant reduction effect of total plate count on tomatoes was achieved by packaging with BC membrane, especially for cracked tomatoes. The cracked tomatoes without packaging became moldy on 21 days, while those packaged with BC membrane did not. The total plate count of cracked tomatoes with BC membrane packaging was reduced by more than 60%.

**Keywords:** bacterial cellulose, glycerol, water vapor transmission rate, tensile strength, weight loss, total plate count, tomatoes preservation.

## 1. Introduction

In response to the climate change crisis, governments around the world have formulated relevant bills and policies, hoping to regulate the use of plastic materials. Therefore, using sustainable materials to replace disposable plastics has become a way to achieve environmental protection and carbon reduction goals. Bacterial cellulose (BC) is mainly an extracellular secondary metabolite produced by acetic acid bacteria fermentation, and it is a straight-chain structural molecule composed of β-D-glucose combined with β-1,4 glycoside chains [1]. It is currently known as the finest natural fiber, the main difference from plant fiber is that BC does not contain hemicellulose, lignin, pectin, and other cell wall components. The bio-based cellulose content is as high as 95% as a kind of high purity and high crystallinity material [2, 3]. Because of its unique properties such as biodegradability, good biocompatibility, high water retention, and high mechanical strength, it is widely used in food processing, health foods, textiles, conductive materials, skin care products, tissue engineering, and wound dressings to have broad application prospects [4, 5]. Besides, BC is also a bio-based sustainable material with promising market potential in packaging [6]. To investigate the production and structure of BC produced by acetic acid bacteria fermentation by culture medium components and culture conditions because the structure of BC and its application are closely related. The scanning electron microscopy images, water vapor transmission rate, and tensile strength of the resulting BC materials were analyzed. Further, the weight loss, moisture content, and total plate count of the fruit to evaluate the feasibility of the resulting BC as a sustainable material applied in food preservation.

## 2. Materials and Methods

### 2.1 Microorganism and media

*Komagayaeibacter xylinus* was cultured in Hestrin-Schramm (HS) medium, consisting of 20 g/L glucose, 5 g/L yeast extract, 5 g/L tryptone, 2.7 g/L $Na_2HPO_4$, and 1.05 g/L citric acid, under static condition at 30℃.

## 2.2 BC production

*K. xylinus* was cultured in HS medium with the extra addition of 1, 2, 3, and 4% glycerol for 9 days, and without glycerol addition as a control group. The resulting BC after washing to removal the broth until the pH was neutral. The washed BC was dried and weighted. BC production was calculated using Eq. (1).

$$\text{BC production } (\tfrac{mg}{L}) = \frac{W}{V} \quad (1)$$

where W (mg) is the dry BC weight and V is the working volume of the medium.

## 2.3 BC characterization analysis

The BC dry membrane was sealed on the mouth of a 15-mL glass tube containing 3 mL of RO water at room temperature. The weight of the entire glass tube was measured at different intervals. The water vapor transmission rate (WVTR) was calculated using Eq. (2), as follow:

$$\text{WVTR } (\tfrac{g}{m^2 \cdot day}) = \frac{\Delta w}{(\Delta t \times A)} \quad (2)$$

where $\Delta w / \Delta t$ (g/day) is the weight change ($\Delta w$) of the entire glass tube within the time ($\Delta t$). A (m$^2$) is the test area of the BC film at the glass tube mouth.

Tensile strength and scanning electron microscopy image (SEM) of the dry BC membrane was analysed by universal testing machine (Model 5965, Instron, USA) and scanning electron microscopy (JEOL, Tokyo, Japan).

## 2.4 Tomatoes preservation evaluation

The BC membrane was used to package non-cracked tomatoes and cracked tomatoes by wrapping method. BC film was used to package non-cracked tomatoes and cracked tomatoes by wrapping method. Tomatoes were stored at room temperature for 28 days, and weight loss, total plate count, and tomato appearance were measured every 7 days.

## 2.5 Determination of tomatoes' weight loss percentage and total plate count

The weight loss percentage was calculated using Eq (3) [7], as follow:

$$\text{Weight loss percentage } (\%) = \frac{(m_1 - m_2)}{m_1} \times 100\% \quad (3)$$

where $m_1$ and $m_2$ are the tomatoes weight (g) at $t_1$ and $t_2$ (days) of storage, respectively.

The surface of the tomato was washed by RO water and the washing solution was collected. Then, the washing solution was spread on a sterile Petri dish containing PCA media and put into an incubator at $30 \pm 1°C$ for 48 h. The total plate count (colony forming units/mL, CFU/mL) was calculated using Eq (4) [8], as follow:

$$\text{Total plate count } (\tfrac{CFU}{mL}) = \frac{(\text{number of colonies (CFU)} \times \text{dilution factor})}{\text{volume of culture plated in mL}} \quad (4)$$
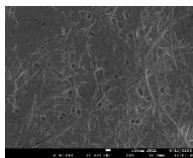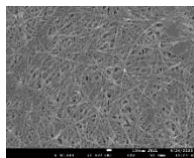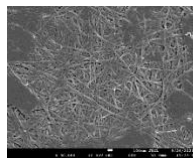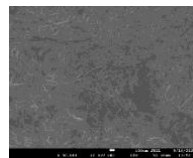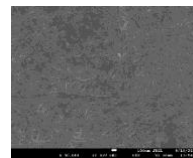
## 3. Results and Discussion

### 3.1. BC production with glycerol addition in HS medium

As shown in Table 1, BC production was improved by adding glycerol. The maximum BC production, BC wet membranes, and tensile strength were obtained as 1% glycerol addition in the HS medium. Compared with the control group (HS medium without adding glycerol), BC production was increased by nearly 1.8-, 1.5-, and 2.8-fold, respectively. In addition, the change of WVTR of BC membranes was opposite to the change of thickness and BC production. When the BC membranes were thicker and the BC production was higher, the WVTR was smaller. It is speculated that when the BC production was increased, there were more fibers in the unit volume of BC, making the pore size and pore volume was relatively small, thus the WVTR of BC was smaller. As shown in Table 2, the appearance of the BC membrane produced by adding 1% glycerol shows that the fibers are thinner than other groups, and the fibers are very densely intertwined.

**Table 1**. The BC production by *K. xylinus* culturing with 0, 1, 2, 3, and 4% glycerol addition in HS medium, and the BC characteristics of the resulting BC.

| Glycerol (%) | pH (initial) | pH (9 days) | BC production (mg/L) | Wet BC membrane thickness (mm) | WVTR (g $H_2O$/cm$^2$/day) | Tensile strength (MPa) |
|---|---|---|---|---|---|---|
| 0 | 4.93 | 3.86 | 1032 | 3.7 | 320.5 | 80.8 |
| 1 | 4.82 | 3.75 | 1855 | 5.7 | 266.8 | 224.5 |
| 2 | 4.86 | 3.82 | 1774 | 5.4 | 274.9 | 176.4 |
| 3 | 5.01 | 3.76 | 1652 | 4.4 | 286.9 | 148.9 |
| 4 | 5.03 | 3.72 | 1594 | 4.3 | 303.2 | 121.2 |

**Table 2**. The SEM image of BC production by *K. xylinus* culturing with 0, 1, 2, 3, and 4% glycerol addition in HS medium, and the BC characteristics of the resulting BC.

| Glycerol (%) | 0 | 1 | 2 | 3 | 4 |
|---|---|---|---|---|---|
| SEM (30 kx) |  |  |  |  |  |

### 3.2. The preservation effects of BC on non-cracked tomatoes

As shown in Fig. 1A and Fig. 1B, when non-cracked tomatoes were packaged in BC, the tomato weight loss and the total plate count on the tomato peel were less, compared with without packaging. Tomatoes without packing started to shrink significantly from the 21 days, while packaged with BC membrane produced by adding 1% glycerol remained the same as the initial (Fig. 1C). In addition, a better preservation effect of the tomatoes packed with BC membrane was produced by adding glycerol, compared with those packaged with the control group (BC produced from the HS medium). When packaged with BC membrane produced by adding 1% glycerol, the weight loss of tomatoes and the total plate count were the least, and tomatoes maintained a better appearance.
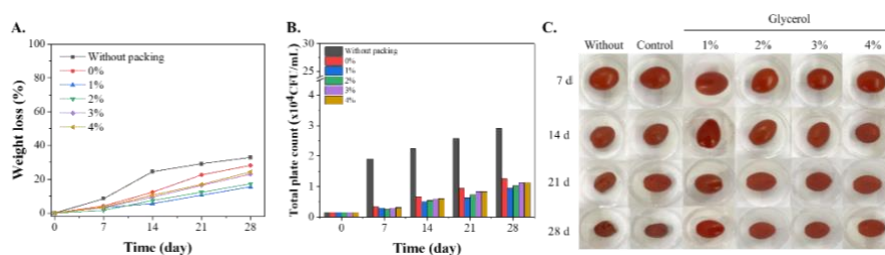


**Fig. 1**. The weight loss (A), total plate count (B), and appearance (C) of non-cracked tomatoes preserved for 28 days using packing by BC produced with 0 (control), 1, 2, 3, and 4% glycerol addition in HS medium, and compared to non-cracked tomatoes with no packaging at room temperature.

### 3.3. The preservation effects of BC on cracked tomatoes

When cracked tomatoes were packaged in BC, the tomato weight loss and the total plate count on the tomato peel were less, compared with without packaging (Fig. 2A and Fig. 2B). Tomatoes without packing started to shrink significantly from the 14 days, while packaged with BC membrane produced by adding 1% glycerol remained similar to the initial (Fig. 2C). In addition, a better preservation effect of the cracked tomatoes packed with BC membrane was produced by adding glycerol, compared with those packaged with the control group (BC produced from the HS medium), especially the differences in appearance of tomatoes. When packaged with BC membrane produced by adding 1% glycerol, the

weight loss of cracked-tomatoes and the total plate count were the least, and tomatoes maintained a better appearance.
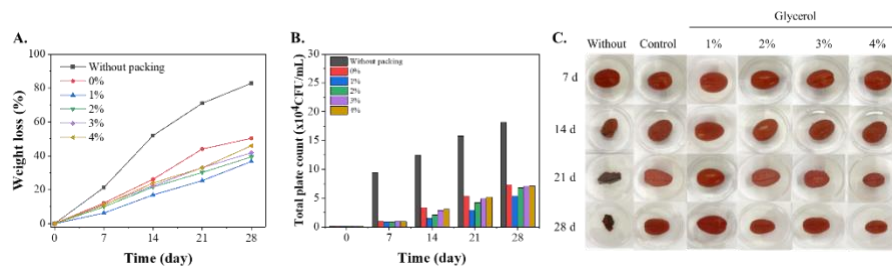


**Fig. 2**. The weight loss (A), total plate count (B), and appearance (C) of cracked tomatoes preserved for 28 days using packing by BC produced with 0 (control), 1, 2, 3, and 4% glycerol addition in HS medium, and compared to non-cracked tomatoes with no packaging at room temperature.

## 4. Conclusion

Both non-cracked and cracked tomatoes packaged in BC film can achieve benefits in reducing tomato weight loss, and decreasing the total plate count. As the thickness of the prepared BC wet film increases, dry BC film packaging performs better in terms of tomato weight loss, and total plate count as freshness indicators. Furthermore, BC is biodegradable and non-toxic, making it environmentally friendly and conducive to sustainable development when applied in food packaging materials. Due to the lower extensibility and transparency of dry BC film, future research can explore ways to enhance BC film extensibility and transparency to improve its convenience in food packaging.

## Acknowledgements

## References

1. A. K. Saleh, H. El-Gendi, N.A. Soliman, W. K. El-Zawawy, Y. R. Abdel-Fattah, "Bioprocess development for bacterial cellulose biosynthesis by novel *Lactiplantibacillus plantarum* isolate along with characterization and antimicrobial assessment of fabricated membrane," *Sci. Rep.*, vol. 12, pp. 2181, 2022.
2. C. Zhong, "Industrial-scale production and applications of bacterial cellulose," Front. Bioeng. Biotechnol., vol. 8, pp. 605374, 2020.
3. N. H. Avcioglu, "Bacterial cellulose: recent progress in production and industrial applications," World J. Microbiol. Biotechnol., vol. 38, no. 5, pp. 86, 2022.
4. S. M. Choi, K. M. Rao, S. M. Zo, E. J., Shin, S. S. Han, "Bacterial cellulose and its applications," Polymers (Basel), vol. 14, no. 6, pp. 1080, 2022.
5. M. Horue, J. M. Silva, I. R. Berti, L. R. Brandão, H. D. S. Barud, G. R. Castro, "Bacterial cellulose-based materials as dressings for wound healing," Pharmaceutics, vol. 15, no. 2, pp. 424, 2023.
6. P. Cazón, M. Vázquez, "Bacterial cellulose as a biodegradable food packaging material: A review," Food Hydrocoll., vol. 113, pp. 106530, 2021.
7. I. Garcia-Orue, E. Santos-Vizcaino, A. Etxabide, J. Uranga, A. Bayat, P. Guerrero, M. Igartua, K. de la Caba, R. M. Hernandez, "Development of bioinspired gelatin and gelatin/chitosan bilayer hydrofilms for wound healing," Pharmaceutics, vol. 11, pp. 314, 2019.
8. H. Desvita, M. Faisal, M. Mahidin, "Natural antimicrobial properties of liquid smoke derived from cocoa pod shells in meatball preservation," S. Afr. J. Chem. Eng. vol. 46, pp. 106-111, 2019.

# Encapsulation of ectoine in lipid nanoparticles for the treatment of inflammatory bowel disease

M. Abajo [1], V. Saez-Martinez **[1]**
[1]I+Med S.Coop.
Albert Einstein, 15. Pab.15, office 117, Vitoria-Gasteiz, Alava, Spain. vsaez@imasmed.com

## Abstract

Inflammatory bowel disease (IBD) is a severe chronic inflammatory disorder of the digestive tract that negatively affects quality of life and requires long-term dependence on effective medications. Thus, in order to facilitate the treatment of this pathology and improve the quality of life of patients, we seek to develop new systems capable of stabilizing the function of the intestinal mucosal barrier. Furthermore, mucoadhesive dosage forms have received substantial attention, as well, as new delivery systems to improve drug bioavailability by prolonging residence time and achieving sustained drug release profiles.

Ectoine molecule becomes of great interest for the treatment of IBD due to its characteristic anti-inflammatory properties. For this reason, a system for encapsulating ectoine in liposomes is proposed. With the purpose of increasing the effectiveness of ectoine in IBD and avoiding possible adverse effects, an ectoine encapsulation system based on liposomes has been designed. In addition, mucoadhesive characteristics are also provided to this system through a coating with chitosan to prolong the local residence time of ectoine and to obtain a sustained release profile, in addition to the antifungal, antimicrobial and immunogenic properties of chitosan, among others.

Once the optimized formulation is obtained, the following characteristics are achieved: an encapsulation efficiency and drug load close to 50%, a particle size of 200 nm for uncoated liposomes and close to 400 nm of coated ones. The coated samples show an ectoine sustained release profile for 7h and a Z potential of 40.3 mV, which indicates that they are nanoparticles with good stability.

**Keywords:** ectoine, encapsulation, liposomes, mucoadhesive, coating, chitosan.

## 1. Introduction

Cases of inflammatory bowel disease (IBD) are becoming more and more common, including Crohn's disease and ulcerative colitis. These are serious chronic inflammatory disorders of the gastrointestinal tract that negatively affect quality of life and require extensive long-term dependence on effective medications, such as mesalazine and other 5-aminosalicylic acids. In this regard, its derivatives are currently considered drugs of choice, while corticosteroids and immunosuppressants are used in more severe cases of IBD [1]. Although these medications are effective, the risk of adverse effects is high, especially considering the chronic and recurring nature of this disease. Furthermore, despite not having a clear pathophysiology, imbalance in the intestinal bacterial ecosystem, impaired intestinal barrier function, and immunological mechanisms play an important role in the development of IBD. For all these reasons, there is a need to develop compounds capable of stabilizing the functioning of the intestinal mucosal barrier, especially to prevent the reappearance of new outbreaks through new, safer therapies. In this regard, the special properties of ectoine for the treatment of IBD make it a compound of great interest in this area [2],[3].

However, despite its suitability in this application, ectoine is considered a small active ingredient, since it is below 500 daltons, and very hydrophilic. This type of compounds are affected by rapid elimination and suboptimal biodistribution. Furthermore, the in vivo efficacy of high polarity molecules, such as this one, may be limited due to their low intracellular absorption. According to this, the encapsulation of drugs in colloidal administration carrier systems represents an improvement in the pharmacokinetics of hydrophilic molecules such as ectoine [4]. These carriers cover a wide range of dispersion systems, such as polymeric nanoparticles, micelles or liposomes, with the aim of protecting the drug against degradation, obtaining a sustained release profile, facilitating the targeted and selective transport of said drug, reducing the side effects and increasing its efficiency since lower doses can be administered [5]. Moreover, mucoadhesive formulations are greatly valued as they can further increase the absorption and bioavailability of the drug.

For this reason, given that ectoine seems to be a promising asset in the treatment of inflammatory bowel disease and that the encapsulation of similar active ingredients in liposomes is effective [6], a system for encapsulating ectoine in liposomes is proposed. In addition, the development of mucoadhesive liposomes thanks to a chitosan coating may become a novel system since no references of ectoine encapsulation in chitosan coated liposomes have been found for this specific therapeutic application.

## 2. Experimental part

### 2.1. Synthesis of liposomes

The polyol method was used to synthesize the liposomes. This method is commonly used because the addition of polyols improves the stability of the dispersion and the phase homogeneity of the bilayer, which is necessary to prevent the drug from diffusing to the outside and to control the sustained release of the active ingredient, thus improving the encapsulation efficiency of the active ingredient [7]. This method involves the preparation of liposomes by premixing a binary lipid/polyol combination, in which the lipid is dissolved or swollen in the polyol, followed by a hydration process.

### 2.2. Coating of liposomes

For the preparation of chitosan-coated ectoine-loaded liposomes, chitosan is dissolved (at desired concentrations) in a 1% acetic acid solution. Next, the chitosan solution is added slowly to the liposome solution under magnetic stirring. The mixture must be kept under stirring for 1h. After this time, the samples should be kept overnight in the refrigerator to stabilize.

## 3. Results and discussion

### 3.1. Liposomes and coated liposomes

The table 1 shows the particle size distribution, polydispersity index (PDI) and zeta potential (ZPot) measured by dynamic light scattering, of a blank sample of empty uncoated liposomes, of ectoine loaded uncoated liposomes (with different ratios to lipid phase), and of ectoine loaded chitosan coated liposomes (with 100% ratio of ectoine load to lipid phase and different percentages of chitosan on the coating). Encapsulation efficiency (EE) and drug load (DL) are also calculated.

**Table 1**: Summary of characteristic properties of blank and ectoine loaded liposomes

| sample | Size (nm) | PDI | ZPot (meV) | EE (%) | DL (%) |
|---|---|---|---|---|---|
| blank | 197 | 0.2 | -43 | - | - |
| Ectoine 12.5% loaded uncoated | 195 | 0.2 | -44 | 45 | 6 |
| Ectoine 25% loaded uncoated | 187 | 0.2 | -48 | 46 | 11 |
| Ectoine 50% loaded uncoated | 197 | 0.2 | -47 | 43 | 21 |
| Ectoine 75% loaded uncoated | 206 | 0.2 | -41 | 51 | 38 |
| Ectoine 100% loaded uncoated | 189 | 0.2 | -44 | 49 | 49 |
| Ectoine 100% loaded coated 0.5% | 373 | 0.4 | 21 | 49 | 49 |
| Ectoine 100% loaded coated 1% | 394 | 0.45 | 38 | 51 | 51 |

The increase of ectoine content does not greatly affect the values of size, PDI or ZPot, compared to blank samples. It does not affect the values of EE, but the DL lineally increases with the ectoine load. This fact indicates that the best formulation is the one with the higher ectoine load, and that is the one selected to develop the chitosan coated samples. These samples show an increase in particle size and PDI, as well as an increase of Zpot to positive values as the amount of chitosan increases. The positive values of ZPot in samples with chitosan content 0.5 and 1% indicate a good coating, and potential good mucoadhesivity.

### 3.2. Controlled release studies

The ectoine release assay from the liposomes (both coated and uncoated liposomes) is carried out in SIF (simulated intestinal fluid) as release medium. The experiments are carried out by placing the ectoine loaded liposomes inside dialysis membranes and they are placed in the SIF medium under sink conditions, with magnetic stirring, at 37ºC, for 48 hours. Aliquots are taken at determined sampling times to measure the ectoine concentration by liquid chromatography (HPLC).
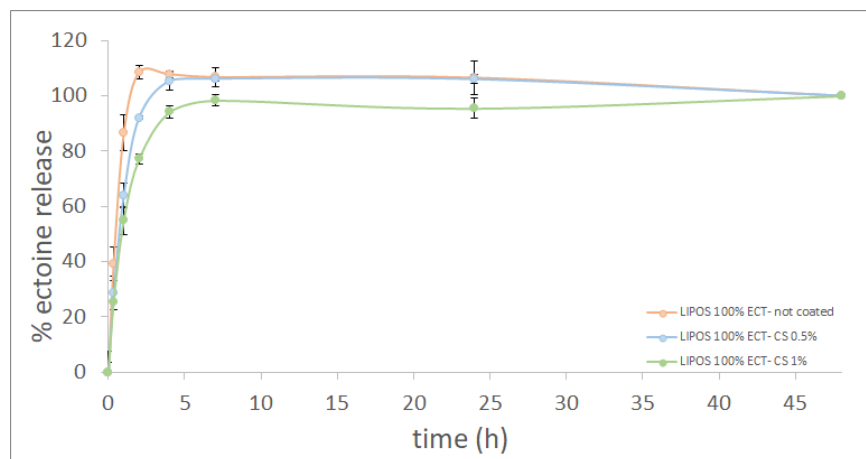
**Fig. 1**: Controlled release profiles of ectoine from liposomes with a 100% ectoine load with respect to the lipid phase (w/w), uncoated (orange) and coated with 0.5% (blue) and 1% (green) chitosan.

The results showed in the graph, indicate that in the case of uncoated liposomes, the maximum percentage of ectoine released is reached after 2 hours of testing, while in the case of coated liposomes, this maximum is reached between 4 and 7 hours of testing. Therefore, it is corroborated that chitosan coating delays the release of ectoine from the liposomes and that a more sustained release profile is obtained than in the case of uncoated liposomes. It is also observed that the higher the concentration of chitosan in the coatings, the more delayed and sustained is the release.

## 4. Conclusion

In this document it is evaluated the possibility of using chitosan coated liposomes loaded with ectoine, to be used for the treatment of IBD. The polyol synthesis method seems to be a robust, potentially scalable method to produce liposomes and the following chitosan coating of the obtained liposomes, can perform two functions: to get a better controlled release profile of the active ectoine molecule, and to provide mucoadhesive properties to the intestinal tissues. This will potentially increase the bioavailability of the drug and the effectiveness of the therapeutic treatment.

## Acknowledgements

## References

1. E. Carty, D. S. Rampton, Evaluation of new therapies for inflammatory bowel disease. British J. Clinic.Pharmacol. vol.56, no 4, pp.351–361, 2003.
2. L. Bethlehem, G. van Echten-Deckert, « Ectoines as novel anti-inflammatory and tissue protective lead compounds with special focus on inflammatory bowel disease and lung inflammation ». Pharmacol. Res., vol.164, pp.105389. 2021.
3. H. Abdel-Aziz, W. Wadie, D. M. Abdallah, G. Lentzen, M. T. Khayyal, Novel effects of ectoine, a bacteria-derived natural tetrahydropyrimidine, in experimental colitis. Phytomedicine, vol. 20, no 7, pp.585–591. 2013.
4. J. O. Eloy, M. Claro de Souza, R. Petrilli, J. P. A. Barcellos, R. J. Lee, J. M. Marchetti, Liposomes as carriers of hydrophilic small molecule drugs: Strategies to enhance encapsulation and delivery. Coll. Surf. B: Biointerfaces, vol. 123, pp.345–363. 2014.
5. G. Barratt, Editorial. Int. J. .Pharm. vol. 454, no 2, pp. 597–598. 2013.
6. M. Przybylo, M. Langner, T. Borowik. High-efficiency encapsulation of hydrophilic compounds in unilamellar liposomes. WO 2018/172504 A1. September 27, 2018.
7. K. Ohishi, K. Tsuchiya, T. Ogura, A. Ebisawa, A. Sekine, Y. Masubuchi, M. Akamatsu, K. Sakai, M. Abe, H. Sakai, Effect of polyol type on the structure and properties of lecithin liposomes prepared using the polyol dilution method, Coll. Surf. A: Physicochemical and Engineering Aspects, vol. 656, Part B, pp. 130509. 2023.

# Mechanical Characterization of Electrospun Tubular Scaffolds with PLA/PCL Bicomponent Fibers

J. Oztemur [1,*], S. Ozdemir [1], H. Sezgin [1], I. Yalcin-Enis [1]

[1] Textile Engineering, Istanbul Technical University, Istanbul, Turkey

**Abstract**

Cardiovascular diseases pose a global health challenge, emphasizing the need for innovative solutions to address compromised blood vessels. This study investigates small caliber tubular scaffolds with bicomponent polylactic acid (PLA) and polycaprolactone (PCL) fibers, focusing on compliance and burst pressure. Coaxial electrospinning is employed to create core-shell fibers, combining the biocompatibility and strength of PLA with the flexibility and long biodegradation rates of PCL. The research aims to assess the suitability of these scaffolds for vascular applications, providing insights into their mechanical behaviors and contributing to the refinement of graft designs. This study contributes to advancing the understanding of vascular graft mechanics, potentially enhancing the success rates of cardiovascular interventions.

**Keywords:** vascular graft, coaxial electrospinning, bicomponent fiber, burst pressure, compliance

## 1. Introduction

Cardiovascular diseases remain a significant global health challenge, highlighting the imperative for innovative solutions to address compromised blood vessels [1]. While autologous vessels, notably the saphenous vein, have long been considered the optimal choice for bypass and revascularization procedures, challenges such as underlying diseases, trauma, anatomical anomalies, size disparities, or previous harvesting hinder their widespread application [2]. This has underscored the increasing importance of artificial vascular transplantation. Modern tissue engineering advancements enable the development of vascular scaffolds to address this need. Vascular grafts are emerging as a promising alternative for replacing damaged vessels due to their minimal infection risk, ease of production, and customizable dimensions and morphology [3]. Optimizing the mechanical properties of vascular grafts is paramount for achieving successful clinical outcomes, improving patient quality of life, and overcoming challenges associated with vascular diseases and bypass procedures [4]. The mechanical properties of vascular grafts, including compliance, burst pressure, and overall structural integrity, are crucial determinants of their functionality and long-term success *in-vivo*. Compliance, defined as the ability of a graft to expand and contract in response to changes in blood pressure, is essential for maintaining physiological hemodynamics and preventing complications such as thrombosis and anastomotic failure. Burst pressure, another critical parameter, reflects the graft's resistance to rupture under pressure, directly influencing its safety and durability in high-pressure arterial environments [1].

Advances in biomaterial selection and scaffold design contribute significantly to the development of vascular grafts with tailored mechanical characteristics, bringing us closer to realizing highly effective and durable vascular replacements [5]. Polylactic acid (PLA) and polycaprolactone (PCL) are noteworthy materials in this context, with PLA offering biocompatibility, biodegradability, and mechanical strength, while PCL contributes prolonged degradation, flexibility, and ductility. The electrospinning method, with its ability to precisely control fiber diameter and alignment, is instrumental in mimicking the intricate architecture of the native extracellular matrix [6]. One notable technique is coaxial electrospinning, which allows for the precise fabrication of bicomponent fibers, enabling us to harness the advantages of both polymers synergistically. Coaxial electrospinning involves the simultaneous extrusion of two different polymers through separate concentric nozzles, resulting in fibers with a core-shell structure. The core-shell structure of bicomponent fibers allows for the integration of desirable properties from each polymer, addressing limitations associated with single-component materials [7].

In this study, the mechanical behaviors of small caliber tubular scaffolds with bicomponent PLA and PCL fibers are investigated. The investigation delves into the influence of polymer type in the core and shell components of these bicomponent fibers. The goal is to comprehensively assess the suitability of these scaffolds for vascular applications, considering not only their structural integrity but also their ability to mimic the mechanical properties

essential for optimal blood flow regulation. The outcomes of this research hold promise for advancing the understanding of vascular graft mechanics, contributing to the refinement of graft designs, and ultimately enhancing the success rates of cardiovascular interventions.

## 2. Materials and Methods

## 2.1. Materials

The neat and the blended state of PCL (with a molecular weight of 80,000) and PLA (with a molecular weight of 230,000) are dissolved in a solvent mixture consisting of chloroform, acetic acid, and ethanol, with an 8:1:1 weight ratio, resulting in a concentration of 8% w/w. All the polymers and chemicals used in this process are procured from Sigma Aldrich. The blending ratio selected for the PCL/PLA solution is set at 50/50.

## 2.2. Methods

*Coaxial electrospinning of tubular scaffolds*

To produce fibrous vascular prostheses with 6 mm diameters through coaxial electrospinning, neat PCL and PLA solutions are employed individually in either the core or shell section (designated as PCL_PLA and PLA_PCL). Additionally, the PCL/PLA blend is exclusively utilized in the core region of bicomponent fibers (referred to as PCLPLA_PCL and PCLPLA_PLA). The coaxial needle comprises inner and outer needles with respective inner diameters of 0.6 and 0.8 mm. A rotational speed of 200 rpm is set for the collector to ensure the creation of randomly distributed bicomponent fibers. Both the core and shell solutions are dispensed at a rate of $1\pm0.1$ mL/h and exposed to a voltage of $9\pm0.5$ kV for 40 minutes to generate scaffolds with adequate wall thickness for subsequent mechanical assessments. The fabrication process is conducted at a temperature of $25\pm2°C$ with a relative humidity of $70\pm5\%$.

*Wall thickness*

The Standard Gage Electronic External Micrometer (Hexagon Metrology, Turkey) is used to gauge the wall thickness of tubular grafts.

*Burst pressure and compliance*

In collaboration with Inovenso (Turkey), a testing apparatus adhering to ISO 7198:2016 standard is designed to measure burst pressure and compliance in this study. Tubular samples, cut into 4 cm segments, undergo burst pressure testing by threading a highly elastic balloon through them. Burst pressure is recorded as the sample expands under pressure, with the test repeated three times for each graft to ensure reliability. For compliance testing, pulsatile intraluminal pressure within the 80-120 mmHg range is generated using a syringe pump. A camera system captures images of the samples at different pressure levels, and automatic diameter measurements are obtained. Compliance values calculated using Equation (1) to assess diameter changes for a 100 mmHg increment, are derived from three repetitions per vascular graft, ensuring robust results.

$$\%\text{compliance} = \frac{\frac{R_{p_2} - R_{p_1}}{R_{p_1}}}{p_2 - p_1} \times 10^4 \qquad (1)$$

Here, $R_{p_2}$ represents the pressurized radius at diastolic pressure in millimeters, $R_{p_1}$ corresponds to the pressurized radius at systolic pressure in millimeters, $p_1$ denotes diastolic pressure in mmHg, and $p_2$ signifies systolic pressure in mmHg.

## 3. Results

## 3.1. Wall thickness

The scaffolds exhibit adequate wall thickness values suitable for mechanical testing and can serve as layers in multilayer graft designs, mimicking the tunica intima. The tubular scaffolds possess a wall thickness of $110.58\pm8.18$ μm, consistent with existing literature [8]. However, if required, the wall thickness can be customized by altering the production time.

## 3.2. Burst pressure and compliance

Table 1 illustrates that samples incorporating PLA in the core segment (PLA_PCL and PCLPLA_PCL) exhibit higher burst strength values compared to those with PCL in the core region (PCL_PLA and PCLPLA_PLA). While the burst pressure of the samples with a core part of PCLPLA blend is 840 mmHg for the shell part of PLA, this value is 629 mmHg for the shell part of PCL. Increasing the PLA proportion throughout the scaffold leads to a noticeable rise in burst strength, coming cross to the optimal requirements for vascular grafts outlined by Johnson et al. in 2019, which recommend a burst strength exceeding 1000 mmHg [9]. The burst pressure that develops due to the core part is related to the high mechanical strength of PLA [1]. Furthermore, the incorporation of PCLPLA blends in the core region enhances the burst strength of the scaffolds when compared to their neat PLA-core counterparts. For instance, PLA_PCL demonstrates a burst strength of 846 mmHg, while PCLPLA_PCL shows a value of 918 mmHg.

**Table 1.** Burst pressure and compliance values of the tubular scaffolds

| Sample | Burst Pressure (mmHg) | Compliance (%/100mmHg) |
|---|---|---|
| PCL_PLA | 629.33 ± 36.33 | 2.67 ± 0.17 |
| PLA_PCL | 846.66 ± 68.85 | 2.01 ± 0.34 |
| PCLPLA_PLA | 840.00 ± 53.78 | 2.55 ± 0.77 |
| PCLPLA_PCL | 918.66 ± 86.77 | 1.49 ± 0.46 |

Native arteries display substantial elasticity at lower pressure levels, but this elasticity decreases with increasing pressure [10]. As compliance and burst strength have an inverse relationship, an effective graft design requires adequate flexibility to mimic the mechanical response of native arteries under pulsatile blood pressure while simultaneously withstanding hemodynamic forces [11]. Hence, it is noticed that fibers with a PCL core result in more compliant tubular scaffolds while PLA addition in the core enhances the burst pressure. Additionally, the use of the PCLPLA blend in the core region develops the compliance of vascular grafts compared neat PLA core. On the other hand, PCL_PLA has the highest compliance with 2.67%/100 mmHg due to the flexible PCL in the inner part. Compliance values are achieved in the range of 1.49–2.67%/100 mmHg and are considered promising for human saphenous vein compliance criteria [12]. Matching compliance minimizes flow disruptions, reducing recirculation, flow separation, and low wall shear stress. This stress triggers vasoactive substances, gene activation, protein expression, and rearrangement, promoting intimal hyperplasia. Therefore, aligning synthetic graft compliance with native arteries improves long-term success by averting flow disruptions and intimal hyperplasia stimuli [13].

## 4. Conclusion

In conclusion, scaffold compositions incorporating PLA in the core segment demonstrate superior burst strength for vascular grafts, notably surpassing those with PCL cores. The PCLPLA blend, particularly in PCLPLA_PCL, exhibits impressive burst pressures exceeding 918 mmHg, aligning with optimal requirements. Scaffold compliance, enhanced by PCL cores, ranges from 1.49% to 2.67%/100 mmHg, meeting human saphenous vein criteria. Matching synthetic graft compliance with native arteries improves long-term success, reducing flow disruptions and intimal hyperplasia stimuli. These findings offer insight into scaffold design for effective vascular tissue engineering applications.

## Acknowledgements

## References

1. Ozdemir, S., Oztemur, J., Sezgin, H., & Yalcin-enis, I. (2023). Optimization of Electrospun Bilayer Vascular Grafts through Assessment of the Mechanical Properties of Monolayers. *ACS Biomaterials Science and Engineering*. https://doi.org/10.1021/acsbiomaterials.3c01161
2. Qiu, S., Du, J., Zhu, T., Zhang, H., Chen, S., Wang, C., Chen, D., & Lu, S. (2023). Electrospun compliant

heparinized elastic vascular graft for improving the patency after implantation. *International Journal of Biological Macromolecules*, 253(P1), 126598. https://doi.org/10.1016/j.ijbiomac.2023.126598

3. Abruzzo, A., Fiorica, C., Palumbo, V. D., Altomare, R., Damiano, G., Gioviale, M. C., Tomasello, G., Licciardi, M., Palumbo, F. S., Giammona, G., & Lo Monte, A. I. (2014). Using polymeric scaffolds for vascular tissue engineering. *International Journal of Polymer Science*, 2014. https://doi.org/10.1155/2014/689390

4. Gao, J., Chen, S., Tang, D., Jiang, L., Shi, J., & Wang, S. (2019). Mechanical Properties and Degradability of Electrospun PCL/PLGA Blended Scaffolds as Vascular Grafts. Transactions of Tianjin University, 25(2), 152–160. https://doi.org/10.1007/s12209-018-0152-8

5. Ozdemir, S., Yalcin-enis, I., Yalcinkaya, B., & Yalcinkaya, F. (2022). An Investigation of the Constructional Design Components Affecting the Mechanical Response and Cellular Activity of Electrospun Vascular Grafts. *Membranes*, 12(929).

6. Oztemur, J., & Yalcin-Enis, I. (2021). Development of biodegradable webs of PLA/PCL blends prepared via electrospinning: Morphological, chemical, and thermal characterization. *Journal of Biomedical Materials Research - Part B Applied Biomaterials,* 109(11), 1844–1856. https://doi.org/10.1002/jbm.b.34846

7. Kareem, M. M., Hodgkinson, T., Sanchez, M. S., Dalby, M. J., & Tanner, K. E. (2019). Hybrid core-shell scaffolds for bone tissue engineering. *Biomedical Materials (Bristol)*, 14(2), 25008. https://doi.org/10.1088/1748-605X/aafbf1

8. De Valence, S., Tille, J. C., Giliberto, J. P., Mrowczynski, W., Gurny, R., Walpoth, B. H., & Möller, M. (2012). Advantages of bilayered vascular grafts for surgical applicability and tissue regeneration. *Acta Biomaterialia*, *8*(11), 3914–3920. https://doi.org/10.1016/j.actbio.2012.06.035

9. Johnson, R., Ding, Y., Nagiah, N., Monnet, E., & Tan, W. (2019). Coaxially-structured fibres with tailored material properties for vascular graft implant. *Materials Science and Engineering C*, *97*(October 2018), 1–11. https://doi.org/10.1016/j.msec.2018.11.036

10. Montini-Ballarin, F., Suárez-Bagnasco, D., Cymberknop, L. J., Balay, G., Caracciolo, P. C., Negreira, C., Armentano, R. L., & Abraham, G. A. (2017). Elasticity response of electrospun bioresorbable small-diameter vascular grafts: Towards a biomimetic mechanical response. *Materials Letters*, *209*, 175–177. https://doi.org/10.1016/j.matlet.2017.07.110

11. Fernández-colino, A., Wolf, F., Rütten, S., Schmitz-rode, T., Rodríguez-cabello, J. C., Jockenhoevel, S., & Mela, P. (2019). *Small Caliber Compliant Vascular Grafts Based on Elastin-Like Recombinamers for in situ Tissue Engineering*. *7*(November), 1–13. https://doi.org/10.3389/fbioe.2019.00340

12. Nezarati, R. M., Eifert, M. B., Dempsey, D. K., & Cosgriff-Hernandez, E. (2015). Electrospun vascular grafts with improved compliance matching to native vessels. *Journal of Biomedical Materials Research - Part B Applied Biomaterials*, *103*(2), 313–323. https://doi.org/10.1002/jbm.b.33201

13. Sarkar, S., Salacinski, H. J., Hamilton, G., & Seifalian, A. M. (2006). The Mechanical Properties of Infrainguinal Vascular Bypass Grafts: Their Role in Influencing Patency. *European Journal of Vascular and Endovascular Surgery*, *31*(6), 627–636. https://doi.org/10.1016/j.ejvs.2006.01.006